

# Vibration-based identification of mechanical properties of orthotropic arbitrarily shaped plates: numerical and experimental assessment

G. Battaglia<sup>1</sup>, A. Di Matteo<sup>2</sup>, G. Micale<sup>3</sup>, A. Pirrotta<sup>4,5</sup>

<sup>1,2,4</sup>Dipartimento di Ingegneria Civile, Ambientale, Aerospaziale, dei Materiali (DICAM),  
Università degli Studi di Palermo, Viale delle Scienze I-90128 Palermo, Italy.

<sup>1</sup>E-mail: [giuseppe.battaglia03@unipa.it](mailto:giuseppe.battaglia03@unipa.it)

<sup>2</sup>E-mail: [alberto.dimatteo@unipa.it](mailto:alberto.dimatteo@unipa.it)

<sup>4</sup>E-mail: [antonina.pirrotta@unipa.it](mailto:antonina.pirrotta@unipa.it)

<sup>3</sup>Dipartimento della Innovazione Digitale ed Industriale  
Università degli Studi di Palermo, Viale delle Scienze I-90128 Palermo, Italy.

<sup>3</sup>E-mail: [giorgiod.maria.micale@unipa.it](mailto:giorgiod.maria.micale@unipa.it)

<sup>5</sup>Department of Mathematical Sciences  
University of Liverpool, Liverpool, UK

<sup>5</sup>E-mail: [antonina.pirrotta@liverpool.ac.uk](mailto:antonina.pirrotta@liverpool.ac.uk)

Corresponding author: Prof. Antonina Pirrotta

Keywords: Material parameter identification; pb-2 Rayleigh-Ritz approach; Particle-Swarm Optimization; Vibration test; Experimental analysis

## Abstract

An innovative procedure is introduced for the identification of the mechanical parameters of orthotropic plates of arbitrary shape, under various boundary conditions, based on free-vibration data. The method employs a combination of a convenient Rayleigh-Ritz approach and Particle-Swarm Optimization to estimate elastic constants of the orthotropic material in a straightforward manner, without requiring computationally demanding iterative Finite Element analyses. Specifically, the pb-2 Rayleigh-Ritz procedure is extended and applied to deal with orthotropic plates, simplifying the approach to more easily treat generic plate shapes, taking advantage of the Green's theorem. The method is then appropriately combined with the Particle-Swarm Optimization procedure to expeditiously identify material parameters based on available free-vibration data. Several numerical applications are presented to show the reliability of the approach, and comparisons with pertinent results available in the literature demonstrate the efficiency and accuracy of the proposed procedure. The study is then supplemented by experimental tests developed in the Laboratory of Experimental Dynamics at the University of Palermo, Italy. In this context, because of the obvious relevance for modern additive manufacturing processes, free-vibration tests are performed on several 3D printed stiffened plates. Numerical vis-à-vis experimental data are examined, showing that the proposed procedure accurately capture equivalent orthotropic parameters of the stiffened plates.

# 1 Introduction

Thin plates and membranes are widely used in many engineering fields, including civil, mechanical and chemical engineering [1]-[3]. In many practical cases, structural properties of these systems differ in two mutually perpendicular directions, so that the plate is described as orthogonally anisotropic or, in short, orthotropic [4]. Such anisotropy can be due to the inherent orthotropic characteristic of the material, or it can be introduced by ribs, corrugation or stiffeners, generally referred to as structural orthotropy [1]-[2]. Examples include plates reinforced with set of equidistant stiffeners in one or two directions, open gridworks and corrugated plates [5]. It is worth noting that, interest in orthotropic plate analysis lies also for instance in the frequent occurrence of these materials in laminae of composite plates, or in the possibility, in some cases, of analytically modeling the whole composite plate as an orthotropic one [6]. Further, even isotropic plates altered by metallurgical process along perpendicular directions exhibit orthotropic characteristics [6]-[7], thus requiring an orthotropic plate model. Additionally, renewed interest has been devoted to classical plate analysis, since procedures developed for these structures are often applicable with minor changes, for instance, to modern laminated plates made of so-called functionally graded materials [8]-[10].

In this context, the problem of the dynamic response determination of orthotropic plates under various boundary conditions (BCs) arises naturally. Thus, considerable attention has been devoted by researchers to developing efficient and accurate methods for the vibration analysis of such systems. In this regard, existing approaches pertain generally rectangular shaped plates and they resort either to Rayleigh-Ritz procedures [11]-[12] or classical Finite Elements (FE) methods [13]. A recent contribution in this field can be found in [6], where exact solutions have been obtained for the free-vibration response of rectangular plates with simply supported or clamped edges, while other numerical approaches can be found in [14]- [16]. On the other hand, the free-vibration analysis of orthotropic generally shaped plates has been much less addressed. Specifically, few common cases have been studied in the literature, such as elliptical or circular plates [17], general triangular plates [18], skew plates [19], and trapezoidal plates [20].

A related problem of considerable engineering interest pertains to the determination of the elastic constants of the orthotropic material, which is clearly fundamental for any structural analysis, optimum design and quality control. Besides classical static testing [21], which can be time consuming and can damage the tested material, an alternative approach combines vibration testing and numerical methods. Specifically, natural frequencies and corresponding mode shapes can be obtained from experimental tests, and the elastic constants in the numerical model are updated until the predicted dynamic properties fit the experimental data within a certain tolerance. Notably, this

procedure represents a fast and non-destructive method for the determination of the mechanical properties, and hence several research efforts have focused in past decades on this topic [22]-[25]. Initial approaches commonly employed a Rayleigh-Ritz technique to model the dynamic behavior of a plate, comprising a least-squares method for estimating the elastic constants [22]-[23]. Recent studies, which generally pertain to the application of FE method and novel optimization procedures, such as Genetic Algorithm, may be found in [26]-[33]. Although being very accurate, these latter approaches can be quite cumbersome and computationally demanding to be implemented, since they require time consuming iteration in the FE simulations.

In this paper, a combination of an appropriately extended Rayleigh-Ritz technique and an alternative optimization procedure are introduced to yield the mechanical characteristic of orthotropic arbitrarily shaped plates based on free-vibration data. Specifically, the so-called pb-2 Rayleigh-Ritz procedure [34]-[37][35], commonly used to treat isotropic plates of general shape, is extended to deal with orthotropic plate. In addition, taking advantage of the Green's theorem, involved computationally demanding double integrals in the plate domain are conveniently converted to more simple line integrals over the contour of the plate, thus facilitating the analysis. In this manner, a generalized eigenvalue problem is derived, whose solution directly yields plate natural frequencies and mode shapes. Notably, since matrices appearing in the eigenvalue problem explicitly depend on the elastic constants, this feature can be exploited to obtain the unknown material properties based on free-vibration data. To this end, an appropriate objective function, related to the aforementioned elastic constants, is defined and conveniently minimized via the Particle-Swarm Optimization (PSO) method [38]. This is a population-based approach, inspired by a mathematical description of the swarming of birds, which has proved particularly suitable for optimization procedures pertaining structural mechanics problems [39]-[42]. Further, comparison of numerical simulations results with pertinent data available in the literature are used to assess the accuracy of the proposed approach, considering several plate shapes and BCs. In passing, it is noted that existing approaches to this problem [22]-[33] concern with rectangular shaped plates, due to their widespread diffusion and the required lower computational cost. On the other hand, to the best of authors' knowledge, the case of arbitrary plate shapes, and their influence on the mechanical properties identification, has not been investigated yet. Remarkably, such cases may not be uncommon, since for instance they occur whenever plate edges are not perfectly parallel to the orthotropy axes, assumed to be aligned to the  $x$  and  $y$  axes of the chosen coordinate system.

Furthermore, these analytical/numerical analyses are supplemented by an extensive experimental study undertaken in the Laboratory of Experimental Dynamics at the University of Palermo, Italy. In this regard, because of the obvious relevance for modern additive manufacturing processes, free-

vibrations tests are performed for several rectangular 3D printed plates reinforced by equidistance stiffeners in one direction. Note that, plates are realized through a so-called fuse deposition modeling 3D printer, employing common polylactic acid (PLA) filaments. In this manner, any possible detrimental effect due to bad connections between the plate and the stiffeners is also avoided. Experimentally measured frequencies and mode shapes are obtained using both laser scanning vibrometer and impulsive tests. Additionally, FE models of the real stiffened plates are developed as further reference. The proposed approach is then used to estimate equivalent orthotropic mechanical properties of the tested plates, and comparisons of the corresponding natural frequencies vis-à-vis experimental data and FE results are reported, demonstrating the reliability and accuracy of the proposed procedure.

## 2 Problem definition

Consider a thin orthotropic homogeneous plate of arbitrary shape, density  $\rho$ , contour  $\Gamma$  and uniform thickness  $h$ , as shown in Fig. 1. Assuming the material to be linearly elastic and the orthotropy axes aligned with the  $x$  and  $y$  axes of a Cartesian system in the plane of the middle surface, using the Love-Kirchhoff's hypotheses, the differential equation for the free-vibration of the plate can be written as [2]

$$D_x \frac{\partial^4 w(x, y, t)}{\partial x^4} + 2H \frac{\partial^4 w(x, y, t)}{\partial x^2 \partial y^2} + D_y \frac{\partial^4 w(x, y, t)}{\partial y^4} = \rho h \frac{\partial^2 w(x, y, t)}{\partial t^2} \quad (1)$$

where  $w(x, y, t)$  is the plate displacement in the vertical direction. Further, the parameters  $D_x$ ,  $D_y$ , and  $H$  are the so-called flexural and torsional rigidities which are given in terms of the material properties as

$$D_x = \frac{E_x h^3}{12(1-\nu_{xy}\nu_{yx})}; \quad D_y = \frac{E_y h^3}{12(1-\nu_{xy}\nu_{yx})}; \quad H = D_1 + 2D_t; \quad (2)$$

$$D_1 = \nu_{xy}D_y = \nu_{yx}D_x; \quad D_t = \frac{G_{xy} h^3}{12}$$

in which  $E_x$  and  $E_y$  are the Young's moduli in the  $x$  and  $y$  directions,  $\nu_{xy}$  is the Poisson's ratio,  $G_{xy}$  is the shear modulus and  $\nu_{yx} = \nu_{xy} E_y / E_x$ .

Note that, for plate made of isotropic material, that is  $E_x = E_y = E$  and  $\nu_{xy} = \nu_{yx} = \nu$ , the flexural rigidity is given as  $D_x = D_y = H = Eh^3/12(1-\nu^2)$ . Thus, in this case, the number of independent parameters reduces from four in Eq. (1) to two (Young's modulus and Poisson's ratio).

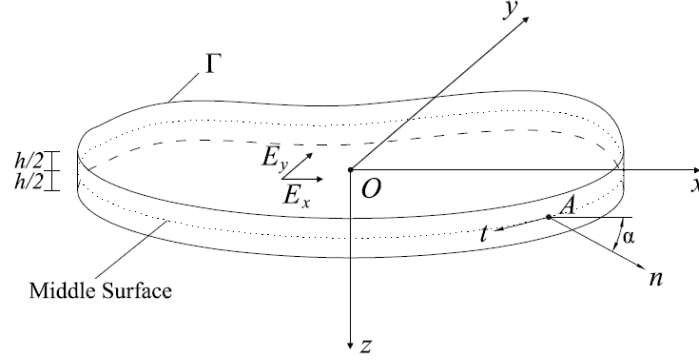


**Figure 1:** Plate of arbitrary shape.

Assuming that the plate undergoes harmonic vibrations,  $w(x, y, t)$  can be approximated as

$$w(x, y, t) = W(x, y)(\beta_1 \cos \omega t + \beta_2 \sin \omega t) \quad (3)$$

Substitution of Eq. (3) into Eq. (1) yields the following partial differential equation in terms of the mode shape  $W(x, y)$  and natural frequency  $\omega$ , as

$$D_x \frac{\partial^4 W(x, y)}{\partial x^4} + 2H \frac{\partial^4 W(x, y)}{\partial x^2 \partial y^2} + D_y \frac{\partial^4 W(x, y)}{\partial y^4} - \rho h \omega^2 W(x, y) = 0 \quad (4)$$

The corresponding maximum strain energy can be expressed as

$$\mathcal{U} = \frac{1}{2} \iint_{\Omega} \left[ D_x \left( \frac{\partial^2 W}{\partial x^2} \right)^2 + 2\nu_{xy} D_y \frac{\partial^2 W}{\partial x^2} \frac{\partial^2 W}{\partial y^2} + D_y \left( \frac{\partial^2 W}{\partial y^2} \right)^2 + 4D_t \left( \frac{\partial^2 W}{\partial x \partial y} \right)^2 \right] dx dy \quad (5)$$

while the maximum kinetic energy is

$$\mathcal{T} = \frac{1}{2} \rho h \omega^2 \iint_{\Omega} W^2 dx dy \quad (6)$$

where  $\Omega$  denotes the generic area of the plate.

Clearly, the pertinent mode shape  $W(x, y)$ , solution of Eq. (4), strongly depends on the chosen plate boundary conditions (BCs). In this regard, let  $n$  and  $t$  be the outward unit normal and tangent vector at a point  $A$  of a generic curvilinear edge of the contour  $\Gamma$ , and denote  $\alpha$  as the angle between the normal  $n$  and the  $x$  axis (see Fig. 1). Omitting the notational dependence of the various variables, for the most common cases the BCs can be specified as

i. Simply-supported edge

$$w = 0 \quad (7.a)$$

$$M_n = 0 \quad (7.b)$$

where  $M_n$  is the normal bending moment applied at the edge, given as

$$M_n = n_x^2 M_x + n_y^2 M_y + 2n_x n_y M_{xy} \quad (8)$$

in which  $n_x$  and  $n_y$  are the components of the unitary vector  $n$  along the  $x$  and  $y$  axes, while the bending moments  $M_x$  and  $M_y$ , and the twisting moment  $M_{xy}$  are specified as

$$M_x = -D_x \left( \frac{\partial^2 w}{\partial x^2} + \nu_y \frac{\partial^2 w}{\partial y^2} \right) \quad (9.a)$$

$$M_y = -D_x \left( \frac{\partial^2 w}{\partial y^2} + \nu_x \frac{\partial^2 w}{\partial x^2} \right) \quad (9.b)$$

$$M_{xy} = -2D_t \frac{\partial^2 w}{\partial x \partial y} \quad (9.c)$$

ii. Clamped edge

$$w = 0 \quad (10.a)$$

$$\frac{\partial w}{\partial n} = n_x \frac{\partial w}{\partial x} + n_y \frac{\partial w}{\partial y} = 0 \quad (10.b)$$

iii. Free edge

$$M_n = 0 \quad (11.a)$$

$$\tilde{V}_n = V_n + \frac{\partial M_{nt}}{\partial s} = 0 \quad (11.b)$$

where  $\tilde{V}_n$  is the so-called effective shear force, while  $M_{nt}$  and  $V_n$  represent the twisting moment and the shearing force on the edge of the plate, given as

$$M_{nt} = (n_x^2 + n_y^2) M_{xy} + n_x n_y (M_y - M_x) \quad M_n = 0 \quad (12.a)$$

$$V_n = n_x V_x + n_y V_y \quad (12.b)$$

in which the shearing forces  $V_x$  and  $V_y$  are

$$V_x = -\frac{\partial}{\partial x} \left( D_x \frac{\partial^2 w}{\partial x^2} + H \frac{\partial^2 w}{\partial y^2} \right) \quad (13.a)$$

$$V_y = -\frac{\partial}{\partial y} \left( H \frac{\partial^2 w}{\partial x^2} + D_y \frac{\partial^2 w}{\partial y^2} \right) \quad (13.b)$$

### 3 pb-2 Rayleigh-Ritz method for general orthotropic plate analysis

In this section the pb-2 Rayleigh-Ritz method, introduced in [34]-[36] for general isotropic plate, is appropriately extended to deal with arbitrarily shaped plates made of orthotropic material. Moreover, taking advantage of the Green's theorem, involved double integrals in the plate domain  $\Omega$  are conveniently converted to more simple line integrals over the contour of the plate  $\Gamma$ .

Specifically, following the classical pb-2 Rayleigh-Ritz method, the function  $W(x, y)$  in Eq. (4)-(6) may be parameterized by

$$W(x, y) = \sum_{j=1}^N c_j \phi_j(x, y) \quad (14)$$

where  $N$  is the chosen truncation limit of the series expansion,  $c_j$  are unknown coefficients to be determined, and  $\phi_j(x, y)$  are the so-called Ritz functions, taken as the product of a boundary function  $\phi_1(x, y)$ , and polynomial functions  $f_j(x, y)$ , that is

$$\phi_j(x, y) = f_j(x, y) \phi_1(x, y), \quad j \geq 2 \quad (15)$$

As far as the boundary function  $\phi_1(x, y)$  is concerned, if the plate BCs vary on the contour  $\Gamma$ , as shown in Fig. 2, it is feasible to appropriately subdivide  $\Gamma$  in the  $N_\gamma$  edges, described by the

equation  $\Gamma_k(x, y)$ , on which the BCs remain constant, that is  $\Gamma = \bigcup_{k=1}^{N_\gamma} \Gamma_k(x, y)$ .

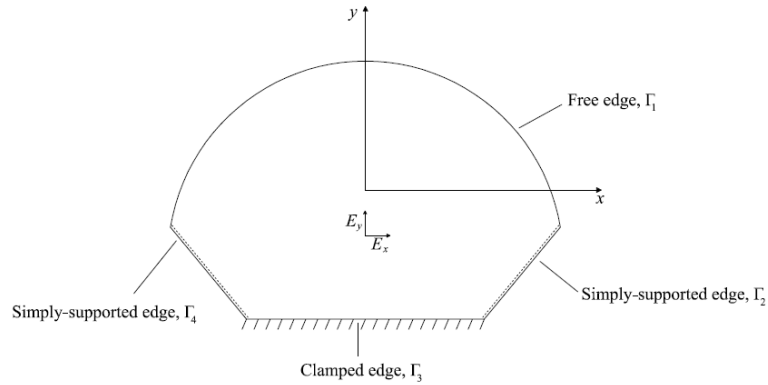


**Figure 2:** Arbitrary shaped plate with mixed BCs and  $N_\gamma = 4$ .

In this manner, the boundary function  $\phi_1(x, y)$  can be expressed as

$$\phi_1(x, y) = \prod_{k=1}^{N_\gamma} \Gamma_k(x, y)^{\beta_k} \quad (16)$$

where the exponents  $\beta_k$  depend on the support edge condition, as

$$\begin{aligned} \beta_k &= 0, & \text{if the } k\text{-th edge is free} \\ \beta_k &= 1, & \text{if the } k\text{-th edge is simply supported} \\ \beta_k &= 2, & \text{if the } k\text{-th edge is clamped} \end{aligned} \quad (17)$$

Further, the polynomial function  $f_j(x, y)$  in Eq. (15) may be generated as

$$f_j(x, y) = x^r y^s \cos^2 \frac{\pi(j-r^2-1)}{2} + x^s y^r \sin^2 \frac{\pi(j-r^2-1)}{2}, \quad j \geq 2 \quad (18)$$

where

$$r = \lceil \sqrt{j-1} \rceil \quad (19)$$

and

$$s = \left( \frac{j-r^2-1}{2} \right) \cos^2 \frac{\pi(j-r^2-1)}{2} + \left( \frac{j-r^2-2}{2} \right) \sin^2 \frac{\pi(j-r^2-1)}{2} \quad (20)$$

in which the symbol  $\lceil \cdot \rceil$  denotes the so-called maximum integer function.

It is worth mentioning that, through the chosen boundary function in Eq. (16), the Ritz functions  $\phi_j(x, y)$  in Eq. (15) automatically satisfy the kinematic BCs.

Introducing the energy functional of the plate

$$\mathcal{F} = \mathcal{U} - \mathcal{T} \quad (21)$$

and applying a Rayleigh-Ritz procedure, that is performing the variation of the functional with respect to the unknown coefficients  $c_j$ , yields

$$\frac{\partial \mathcal{F}}{\partial c_j} = 0, \quad j = 1, \dots, N \quad (22)$$

Substituting Eqs. (5, 6) into Eq. (22), taking into account Eqs. (14)-(20), and manipulating, leads to the generalized eigenvalue problem (see Appendix A for the detailed derivation)

$$(\mathbf{K} - \lambda \mathbf{M})\mathbf{c} = \mathbf{0} \quad (23)$$

where  $\lambda = \rho h \omega^2 / \nu_{xy}$ ,  $\mathbf{c}$  is the vector containing the coefficients  $c_j$ , while  $\mathbf{K}$  and  $\mathbf{M}$  are the stiffness and mass matrices, respectively, which depend on the Ritz functions  $\phi_j(x, y)$ .

Specifically, introducing the matrices  $\mathbf{R}^{(de,pq)}$  whose elements are given as

$$R_{ij}^{(de,pq)} = \iint_{\Omega} \left[ \frac{\partial^{d+e} \phi_i(x, y)}{\partial x^d \partial y^e} \right] \left[ \frac{\partial^{p+q} \phi_j(x, y)}{\partial x^p \partial y^q} \right] dx dy, \quad i = 1, \dots, N; j = 1, \dots, N \quad (24)$$

where the generic superscript  $(de, pq)$  refers to the order of the partial derivatives in Eq. (24)

(see Appendix A), the matrices  $\mathbf{K}$  and  $\mathbf{M}$  can be expressed by

$$\mathbf{K} = \frac{D_x}{\nu_{xy}} \mathbf{R}^{(20,20)} + \frac{D_y}{\nu_{xy}} \mathbf{R}^{(02,02)} + D_y \left[ \mathbf{R}^{(20,02)} + \mathbf{R}^{(02,20)} \right] + 4 \frac{D_t}{\nu_{xy}} \mathbf{R}^{(11,11)} \quad (25)$$

and

$$\mathbf{M} = \mathbf{R}^{(00,00)} \quad (26)$$

Note that in Eqs. (25) and (26) specific values of the generic superscript  $(de, pq)$  have been appropriately substituted in the matrices  $\mathbf{R}^{(de, pq)}$  in Eq. (24), as shown in Appendix A.

Once these matrices have been defined, the eigenvalue problem in Eq. (23) can be solved, leading to the natural frequencies  $\omega$  and the corresponding coefficients vector  $\mathbf{c}$ .

### 3.1 Simplified expression in terms of line integrals

Although Eqs. (23)-(26) provide a simple and effective method to determine natural frequencies and mode shapes of orthotropic plates under most common BCs, double integrals in Eq. (24) can be particularly cumbersome to be evaluated for plates of arbitrary shape. For this reason application of the aforementioned procedure is generally limited to the case of rectangular plate, for which integrals can be simply obtained numerically.

In this context, taking into account Green's theorem, double integrals in Eq. (24) can be converted into much simpler line integrals, which allow for an elegant and straightforward application of the proposed procedure to plates of arbitrary shape.

Specifically, introduce the functions  $A_{ij}^{(de, pq)}(x, y)$  and  $B_{ij}^{(de, pq)}(x, y)$  as

$$A_{ij}^{(de, pq)}(x, y) = \int \left[ \frac{\partial^{d+e} \phi_i(x, y)}{\partial x^d \partial y^e} \right] \left[ \frac{\partial^{p+q} \phi_j(x, y)}{\partial x^p \partial y^q} \right] dx, \quad i=1, \dots, N; j=1, \dots, N \quad (27)$$

and

$$B_{ij}^{(de, pq)}(x, y) = \int \left[ \frac{\partial^{d+e} \phi_i(x, y)}{\partial x^d \partial y^e} \right] \left[ \frac{\partial^{p+q} \phi_j(x, y)}{\partial x^p \partial y^q} \right] dy, \quad i=1, \dots, N; j=1, \dots, N \quad (28)$$

Note that the above defined indefinite integrals can be generally obtained in closed form since they involve integrations of polynomial functions.

Further, let the equation of the  $k$ -th edge  $\Gamma_k(x, y)$  of the plate be given in parametric form as  $\Gamma_k(\gamma) = [x_k(\gamma), y_k(\gamma)]$ . Thus, functions in Eqs. (27) and (28) can be expressed in terms of the generic parameter  $\gamma$  as well, that is  $A_{ij}^{(de, pq)}(\gamma)$  and  $B_{ij}^{(de, pq)}(\gamma)$ .

Taking into account Eqs. (27) and (28), application of the Green's theorem yields the terms  $R_{ij}^{(de, pq)}$  in Eq. (24) as

$$R_{ij}^{(de, pq)} = \frac{1}{2} \sum_{k=1}^{N_\gamma} \int_{\Gamma_k} H_{ij,k}^{(de, pq)}(\gamma) d\gamma \quad (29)$$

where the symbol  $\int_{\Gamma_k}(\cdot) d\gamma$  denotes the classical line integration, and the function  $H_{ij,k}^{(de, pq)}(\gamma)$  is

given as

$$H_{ij,k}^{(de,pq)}(\gamma) = -A_{ij}^{(de,pq)}(\gamma) \frac{dy_k(\gamma)}{d\gamma} + B_{ij}^{(de,pq)}(\gamma) \frac{dx_k(\gamma)}{d\gamma} \quad (30)$$

In this manner, Eq. (29) allows for a simpler evaluation of the terms  $R_{ij}^{(de,pq)}$ , which are involved in the elements of the mass and stiffness matrices in Eqs. (25) and (26), and the proposed procedure can be used even for plates of more complex shape.

In passing, it is noted that if the plate BCs do not vary on the contour  $\Gamma$ , and the entire plate boundary can be described by a single equation  $\Gamma(\gamma)$ , then the line integral in Eq. (29) simply reverts to a contour path integral in  $\Gamma$ , that is

$$R_{ij}^{(de,pq)} = \frac{1}{2} \oint_{\Gamma} H_{ij}^{(de,pq)}(\gamma) d\gamma \quad (31)$$

## 4 Mechanical properties identification

As previously shown, the proposed pb-2 Rayleigh-Ritz approach leads to an eigenvalue problem which can be easily solved to determine natural frequencies, as well as mode shapes, of arbitrarily shaped plates under several BCs and made of orthotropic material.

Notably, one of the beneficial features of this procedure lies in the fact that plate flexural and torsional rigidities directly appear in the mass and stiffness matrices in Eqs. (25) and (26). Thus, it can be argued that the aforementioned approach could be appropriately exploited, as an inverse problem, for the identification of the orthotropic material parameters. Specifically, based on some known values of the natural frequencies  $\tilde{\omega}_k$ , for instance experimentally identified, an inverse procedure can be implemented leading to an estimate of the four involved mechanical parameters  $E_x$ ,  $E_y$ ,  $G_{xy}$  and  $\nu_{xy}$ . Note that, such a procedure can be easily pursued properly defining an objective function, to be minimized, related to the aforementioned elastic constants.

Specifically, assuming dimensions and density of the plate to be known, in this study the considered objective function is expressed by the functional

$$\Phi(D_x, D_y, D_t, \nu_{xy}) = \frac{1}{n_f} \sum_{k=1}^{n_f} \sqrt{\frac{|\tilde{\omega}_k - \omega_k|}{\tilde{\omega}_k}} \quad (32)$$

subject to the constraints

$$\begin{aligned} D_x &\in [D_{x,l}, D_{x,u}]; D_y \in [D_{y,l}, D_{y,u}]; \\ D_t &\in [D_{t,l}, D_{t,u}]; \nu_{xy} \in [\nu_{xy,l}, \nu_{xy,u}] \end{aligned} \quad (33)$$

where  $n_f$  is a chosen number of considered frequencies,  $\omega_k$  is the  $k$ -th natural frequency determined solving the eigenvalue problem in Eq. (23) and the terms in square brackets in Eq. (33)

denote lower and upper bounds, respectively. Therefore, the functional to be minimized gives an account of the deviation between the measured  $\tilde{\omega}_k$  and numerically calculated  $\omega_k$  frequencies. Clearly, minimization of the functional in Eq. (32) leads to estimates of the flexural and torsional rigidities in Eq. (2), since the  $n_f$  natural frequencies  $\omega_k$  depend on these parameters via Eq. (23).

As far as the minimization of the functional  $\Phi(D_x, D_y, D_t, \nu_{xy})$  is concerned, the Particle-Swarm Optimization (PSO) method [38] has been used. This is a population-based approach, inspired by a mathematical description of the swarming of birds, with some useful characteristics [39] as simple implementation and execution, avoided evaluation of the objective function derivatives, and ability of finding regions in which a global minimum is attained even in presence of non-smooth objective functions (as in the case in which experimental data are used). Further, the method is based on few parameters (see [39] for details), among which the maximum number of iterations and the population size are particularly important. In fact, to avoid possible premature convergence of the PSO method, appropriate values of these two parameters can be chosen.

In this context, it is worth mentioning that other optimization procedures could be used to minimize the functional in Eq. (32) with respect to the coefficients  $(D_x, D_y, D_t, \nu_{xy})$ , such as ant colony optimization [43]-[44], genetic algorithms [29]-[31], and hybrid optimization techniques exploiting combination of the above mentioned procedures and classical gradient-based minimization routines [41]. Moreover, objective functions different from the one in Eq. (32) could also be considered, as those reported in [24] and [26], and even some based on the joint use of experimentally determined natural frequencies and mode shapes [45]. In passing, it is noted that, although these approaches may lead to increased accuracy, their influence on the identified parameters is out of the scope of the present study, and therefore they will not be investigated.

As far as the numerical implementation of the identification procedure is concerned, a three steps scheme can be followed:

- i) Based on known plate dimensions, geometry and BCs, matrices  $\mathbf{R}^{(de,pq)}$  in Eqs. (25) and (26) are determined using Eq. (29).
- ii) PSO, implemented for instance in MATLAB environment, is used to minimize the functional in Eq. (32) with respect to the coefficients  $(D_x, D_y, D_t, \nu_{xy})$ . At each iteration of the optimization procedure, values of the aforementioned coefficients are assumed and corresponding natural frequencies  $\omega_k$  are obtained solving the eigenvalue problem in Eq. (23).

iii) Once the optimal values of the coefficients  $(D_x, D_y, D_t, \nu_{xy})$  which minimize Eq. (32) have been obtained, pertinent values of the mechanical parameters can be determined taking into account Eq. (2) as

$$\begin{aligned} E_x &= \frac{12}{h^3} (D_x - D_y \nu_{xy}^2); E_y = \frac{D_y}{D_x} E_x \\ G_{xy} &= \frac{12 D_t}{h^3}; \nu_{yx} = \frac{D_y}{D_x} \nu_{xy} \end{aligned} \quad (34)$$

Observe that the evaluation of the matrices  $\mathbf{R}^{(de,pq)}$ , which represents the most computationally demanding step, can be carried out once beforehand. In this manner, since second and third steps do not depend on the plate shape or BCs, the identification procedure is completely generic and can be implemented independently on the first step.

## 5 Numerical Applications

In this section, the proposed procedure is applied to two plate configurations, previously analyzed in the literature, with different shapes and boundary conditions (see Fig. 3). Specifically, a clamped elliptical plate and a triangular cantilever plate have been analyzed. Further, several material properties have been taken into account for each configuration, demonstrating the ability of the method to detect mechanical properties regardless the orthotropic material considered. In this regard, the mechanical characteristics of the materials employed are reported in Tab. 1.

**Table 1:** Material properties [46]

Material	$E_x$ [GPa]	$E_y$ [GPa]	$G_{xy}$ [GPa]	$\nu_{xy}$	$\rho$ [Kg/m <sup>3</sup> ]
<i>Graphite/Epoxy</i>	181	10.30	7.17	0.28	1600
<i>Carbon/Epoxy</i>	229	13.35	5.25	0.315	1600

Finally, to assess the accuracy of the procedure, proposed method results are compared with pertinent data from the literature, for all the above mentioned cases.

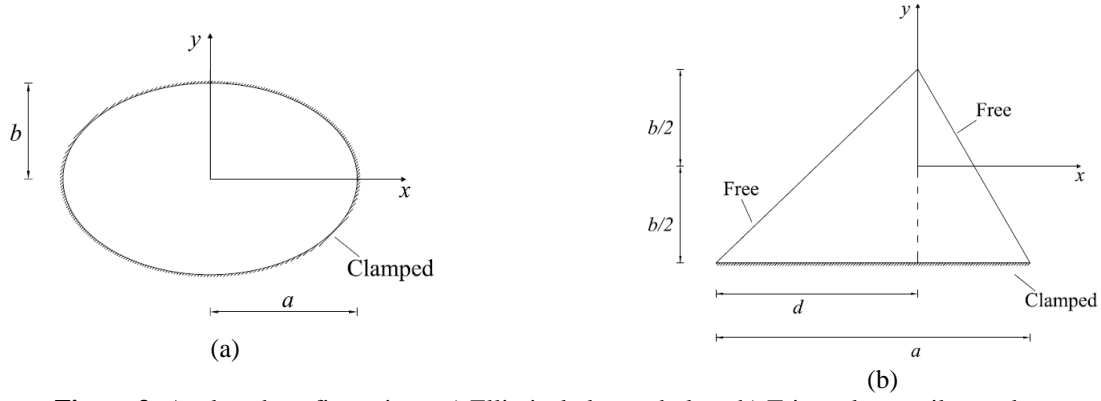


**Figure 3:** Analyzed configurations: a) Elliptical clamped plate; b) Triangular cantilever plate.

Note that, for the following applications upper and lower bounds in Eq. (33) have been determined using Eq. (2) and assuming a  $\pm 60\%$  of variation with respect to the reference values in Tab.1. Further,  $N = 20$  terms in Eq. (14) have been used for the pb-2 Rayleigh-Ritz procedure.

### 5.1 Numerical applications: elliptical plate

Consider the case of an elliptical shaped plate, made of orthotropic material, clamped along the whole boundary, as shown in Fig. 3(a). The boundary equation  $\Gamma(x, y)$  is given as

$$\Gamma(x, y) = \left(\frac{x}{a}\right)^2 + \left(\frac{y}{b}\right)^2 - 1 \quad (35)$$

and, considering the chosen BCs, the boundary function  $\phi_1(x, y)$  in Eq. (16) can be expressed as  $\phi_1(x, y) = \Gamma(x, y)^2$ . Further, taking into account that the boundary of the plate is defined by the curve in parametric form

$$\begin{cases} x = a \cos \gamma \\ y = b \sin \gamma \end{cases}, \quad 0 \leq \gamma \leq 2\pi \quad (36)$$

Eq. (31) can be used to obtain the element of the matrices  $\mathbf{R}^{(de,pq)}$  in Eqs. (25) and (26).

The proposed procedure has been then applied to identify the mechanical characteristics of the two materials in Tab. 1, assuming as measured frequencies  $\tilde{\omega}_k$  in Eq. (32) those numerically calculated in [17] (see Tab. 2), considering  $a = 1m$ ,  $b = 0.5m$  and  $h = 5mm$ .

**Table 2:** Frequencies  $\tilde{f}_k = \tilde{\omega}_k/2\pi$  [Hz] for elliptical plate.

Material	Mode sequence number									
	1 <sup>st</sup>	2 <sup>nd</sup>	3 <sup>rd</sup>	4 <sup>th</sup>	5 <sup>th</sup>	6 <sup>th</sup>	7 <sup>th</sup>	8 <sup>th</sup>	9 <sup>th</sup>	10 <sup>th</sup>
<i>Graphite/Epoxy</i>	22.5	46.2	47.5	73.4	79.9	87.8	110.5	111.8	145.9	151.4
<i>Carbon/Epoxy</i>	25.0	51.5	52.5	80.4	89.8	97.2	121.9	123.2	163.5	168.2

Further, to investigate on the accuracy of the approach, two different number of considered natural frequencies  $n_f$  in Eq. (32) have been used, namely  $n_f = 5$  and  $n_f = 10$ . In this regard, identified mechanical parameters, for each value of  $n_f$  and material, are reported in Tab. 3. Note that, for each identified parameter, the pertinent relative error is reported in square brackets.

**Table 3:** Identified mechanical parameters for elliptical clamped plate

Material	$n_f$	$E_x$ [GPa]	$E_y$ [GPa]	$G_{xy}$ [GPa]	$\nu_{xy}$
<i>Graphite/Epoxy</i>	5	181.7 [0.4 %]	10.34 [0.4 %]	7.39 [3.1 %]	0.201 [28.3 %]
	10	180.8 [0.1 %]	10.23 [0.1%]	7.05 [1.7 %]	0.303 [8.3 %]
<i>Carbon/Epoxy</i>	5	228.5 [0.2 %]	13.32 [0.2 %]	4.36 [16.8 %]	0.411 [30.4 %]
	10	228.8 [0.1 %]	13.34 [0.1 %]	5.12 [2.4 %]	0.336 [5.9 %]

As it can be observed in Tab. 3, a satisfactory agreement between identified and reference Young's moduli in the  $x$  and  $y$  directions have been obtained, even for low number of natural frequencies  $n_f$ . However, generally a higher value of  $n_f$  must be taken into account to more accurately identify the Poisson's ratio and the shear modulus, for both materials considered. This may be due to the fact that natural frequencies are not particularly influenced by variations of  $\nu_{xy}$ .

## 5.2 Numerical application: triangular plate

Consider a general orthotropic triangular plate, bounded by the sides (1)  $y = bx/d + b/2$ , (2)  $y = -b/2$  and (3)  $y = -bx/(a-d) + b/2$ , where the quantities  $a$ ,  $b$  and  $d$  are shown in Fig. 3(b). Assuming the plate to be clamped only along the second edge, while the other two are free, the boundary function  $\phi_1(x, y)$  in Eq. (16) can be expressed as

$$\phi_1(x, y) = \left( y + \frac{b}{2} \right)^2 \quad (37)$$

Representing the aforementioned boundary equations in parametric form, the element of the matrices  $\mathbf{R}^{(de,pq)}$  in Eqs. (25) and (26) can be determined using Eq. (29).

The mechanical characteristics of the two materials in Tab. 1 have been then identified, assuming as measured frequencies  $\tilde{\omega}_k$  in Eq. (32) those numerically calculated in [18] (see Tab. 4), considering  $a = 0.25 \text{ m}$ ,  $b = 3a/2$ ,  $d = a/2$  and  $h = 5 \text{ mm}$ .

**Table 4:** Frequencies  $\tilde{f}_k = \tilde{\omega}_k / 2\pi$  [Hz] for triangular plate.

Material	Mode sequence number									
	1 <sup>st</sup>	2 <sup>nd</sup>	3 <sup>rd</sup>	4 <sup>th</sup>	5 <sup>th</sup>	6 <sup>th</sup>	7 <sup>th</sup>	8 <sup>th</sup>	9 <sup>th</sup>	10 <sup>th</sup>
<i>Graphite/Epoxy</i>	29.6	128.4	218.2	311.8	536.7	572.6	957.9	1606.4	1801.0	1818.2
<i>Carbon/Epoxy</i>	33.7	146.1	1264.8	201.3	507.1	655.4	942.1	1654.1	1817.7	2002.8

In this regard, identified material parameters are reported in Tab. 5, for the two chosen values of  $n_f$ . Note that, for each identified parameter, the pertinent relative error is reported in square brackets.

**Table 5:** Identified mechanical parameters for triangular cantilever plate

Material	$n_f$	$E_x$ [GPa]	$E_y$ [GPa]	$G_{xy}$ [GPa]	$\nu_{xy}$
<i>Graphite/Epoxy</i>	5	163.8 [9.5 %]	10.29 [0.1 %]	7.17 [0 %]	0.226 [19.1 %]
	10	181.0 [0 %]	10.30 [0 %]	7.17 [0 %]	0.279 [0 %]
<i>Carbon/Epoxy</i>	5	216.2 [5.6 %]	13.34 [0.1 %]	5.24 [0.1 %]	0.212 [32.7 %]
	10	229.0 [0 %]	13.35 [0 %]	5.25 [0 %]	0.315 [0 %]

Again, as it can be observed in Tab. 5, a good agreement between identified and reference Young's moduli in the  $x$  and  $y$  directions have been obtained, even for low number of natural frequencies  $n_f$ . However, in this case also a very low value of relative error has been achieved for the shear modulus  $G_{xy}$  for both materials, while higher discrepancies are obtained for the Young modulus  $E_x$ . This could be due to both the shape of the plate and the adopted BCs. Further, it can be observed that considering a higher number of natural frequencies  $n_f$  allow to very accurately estimate all the mechanical characteristics.

As a final remark, results suggest that these particular plate shape and BCs may be better suitable to more precisely identify material parameters, even considering a lower number of natural frequencies, especially in terms of shear modulus and Poisson's ratio.

Once the accuracy of the proposed procedure has been assessed through several numerical applications, in the next section the reliability of the approach will be experimentally investigated. Specifically, based on the so-called Equivalent Plate Model, 3D-printed stiffened plates will be studied as equivalent orthotropic ones, and the proposed procedure will be used to determine the equivalent orthotropic material parameters.

## 6 Experimental validation of the proposed procedure

To further investigate on the reliability and accuracy of the proposed procedure, an extensive experimental campaign has been carried out in the Laboratory of Experimental Dynamics at the University of Palermo, Italy. The investigation has focused on the assessment of the equivalent orthotropic mechanical characteristics of plates reinforced by equidistant grooves stiffeners.

In this regard, it is noted that corrugated and stiffened plates have been deeply investigated in the past decades. Stiffened plates, in fact, show some economical and mechanical advantages, but their

analysis and optimization may be a daunting task, thus requiring computationally demanding FE analyses. In some cases, however, mechanical behavior of stiffened or corrugated plates can be also studied considering an equivalent flat plate made of orthotropic material, generally referred to as Equivalent Plate Model (EPM). Experimental data indicate good accuracy of such idealization, provided that relatively small, and closely spaced, stiffeners are employed. Clearly, this approach yields various advantages, such as reducing the computational effort that FE method would have demanded, especially in preliminary design. Therefore, several research efforts have been devoted to determining the required equivalent orthotropic plate parameters. It is worth noting that, the majority of studies have dealt with the cases of corrugated plates, introducing several different approximate relations, which have been also experimentally analyzed [47]. On the other hand, the case of longitudinally stiffened plates has been less investigated, many studies date back to the 50th [48]-[51] and few other have been more recently presented [52] on this topic. Further, experimental analyses in the literature generally comprise only the first fundamental natural frequency, while the accuracy of such EPM pertaining higher natural frequencies and mode shapes has been much less addressed [51]. Thus, it is apparent the need for up-to-date studies on this field, which could also experimentally assess the accuracy of the EPM even for stiffened plates.

On this base, aiming both at validating the reliability of the proposed procedure and the classical EPM for stiffened plates, present experimental analyses have focused on rectangular longitudinally stiffened plates, taking into account several natural frequencies and mode shapes. Specifically, three different plate configurations have been considered, as reported in Fig. 4(a): a homogeneous flat rectangular plate (Configuration #1), a rectangular plate with 6 equidistant stiffeners in one direction (Configuration #2) and a rectangular plate with 9 equidistant stiffeners in one direction (Configuration #3). A sketch of the plates geometry is shown in Fig. 4(b), while dimensions of each Configuration is reported in Tab. 6.

It is worth mentioning that plates have been realized through a 3D printer Model PRUSA i3 MK2S, as shown in Fig. 4(c), which is a fuse deposition modeling printer, employing common polylactic acid (PLA) filaments. Remarkably, thanks to the 3D printing manufacturing process, any mechanical or adhesive bonding between the plate and the stiffeners have been avoided, thus eliminating any possible detrimental effects due to the connections adopted.

**Table 6:** Plate configurations parameters

Configurations	$\tilde{a}$ [mm]	$\tilde{b}$ [mm]	$h$ [mm]	$\tilde{h}$ [mm]	$\tilde{L}$ [mm]	$\tilde{p}$ [mm]	$\rho$ [Kg/m <sup>3</sup> ]
<b>Configuration #1</b>	190	210	4	-	-	-	1240
<b>Configuration #2</b>	190	210	4	2	7.6	22.8	1240
<b>Configuration #3</b>	190	210	4	2	7.6	15.2	1240

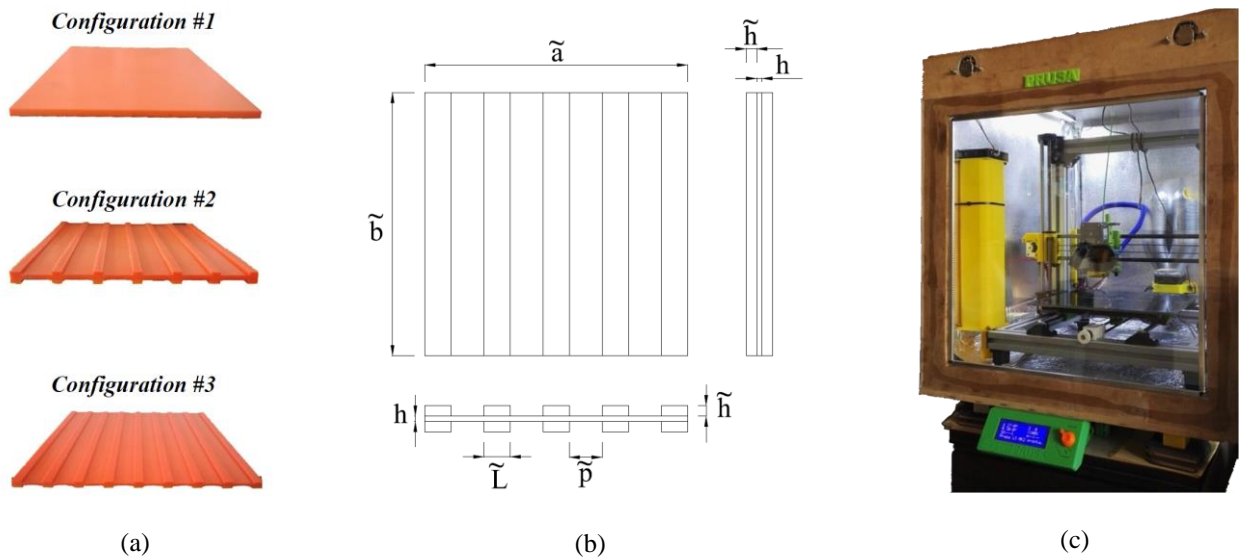


**Figure 4:** (a) Plate Configurations; (b) Plate geometry; (c) 3D Printer.

## 6.1 Experimental set-up and data acquisition

As far as the experimental set-up is concerned, cantilever plate conditions have been employed for the tests for each Configuration, since these BCs are particularly suitable for experiments compared to others common cases. In this regard, Fig. 5 shows the adopted experimental set-up, while in Fig. 6 pictures of the experimental equipments are reported.

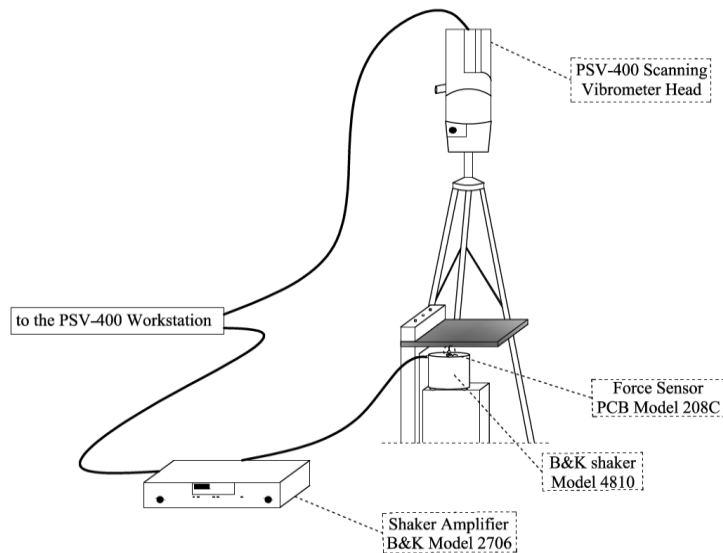


**Figure 5:** Experimental set-up.

As it can be seen, each plate Configuration has been fixed on one side of a rigid frame (Fig. 6(b)) and excitation has been provided through a B&K shaker type 4810 (Fig. 6(c)) connected with a stinger close to the clamped side of the plate. Further, input force signal has been acquired through

a PCB ICP Force Sensor model 208C, directly positioned between the shaker and the plate (Fig. 6 (d)). The Frequency Response Functions (FRFs) and the mode shapes of the plates have been measured with a Polytec laser scanning vibrometer model PSV-400 (Fig. 6(e)) which allow to measure both velocity and displacements of a chosen grid of points of the plate without any contact through the laser signal. Note that the forcing signal, provided by the shaker connected to the B&K amplifier model 2706 Fig. 6(f) is generated by the Polytec workstation Fig. 6(g), to which the laser head is also connected.



**Figure 6:** Devices employed for the experimental tests.

A sweep sine, of frequency range between 0.1 and 2000 Hz, has been used as forcing signal and repeated for each point of the grid, while the chosen sample rate was 2000 Hz. Finally, the mode shapes and corresponding natural frequencies have been identified by means of the vibrometer software version 9.2.

To obtain more precise data especially at the lowest frequency, impulsive tests have been also performed for all the three Configurations. Specifically, a small impact hammer model PCB 086E80 Fig. 7(a) has been used to provide the impulse, while four miniature PCB piezoelectric accelerometers Model 352C23 Fig. 7(b) have been employed to measure the acceleration responses on different points of the plates. Note that, considering the small dimensions and mass of each of these accelerometers, the influence of these sensors on the plate frequency response can be neglected. Further, signals have been then digitalized and acquired by means of a National Instruments NI 4497 PXI Acquisition Board provided inside the chassis of a National Instruments

PXIe model 1082, and then processed in self-developed LabView and MATLAB environments programs (Fig. 7(c)).



(a) (b) (c)

**Figure 7:** Devices employed for the impulsive tests: (a) PCB impact hammer model 086E80; (b) miniature PCB accelerometers Model 352C23; (c) NI PXIe model 1082.

For each plate Configuration five tests have been performed, both with shaker and the impact hammer, and pertinent average FRFs has been determined. The corresponding identified natural frequencies are reported in Tab. 7.

**Table 7:** Experimentally identified frequencies  $\tilde{f}_k = \tilde{\omega}_k / 2\pi$  [Hz]

Configurations	Mode sequence number									
	1 <sup>st</sup>	2 <sup>nd</sup>	3 <sup>rd</sup>	4 <sup>th</sup>	5 <sup>th</sup>	6 <sup>th</sup>	7 <sup>th</sup>	8 <sup>th</sup>	9 <sup>th</sup>	10 <sup>th</sup>
<b>Configuration #1</b>	22.4	60.3	138.7	216	219	388	412	476	545	661
<b>Configuration #2</b>	34.5	76	201	221	292	474	482	586	650	684
<b>Configuration #3</b>	37.4	88.4	218.5	236.2	317.5	506	511	646	700	745

## 6.2 Experimental results vis-à-vis numerical simulations

Once natural frequencies and mode shapes of the three plates have been determined, mechanical parameters of the analyzed Configurations have been identified applying the proposed method. Further, to verify the reliability of the approach, comparison among experimental data, FE simulations and numerical results of the previously introduced procedure has been performed.

Firstly, material parameters (Young's modulus  $E$  and Poisson's ratio  $\nu$ ) of the homogeneous flat plate (Configuration #1), assumed to be isotropic, have been identified minimizing the mean squared error between the first two experimentally obtained natural frequencies, and the corresponding analytical ones reported in [3]. In this regard, the identified values are reported in first line of Tab. 8. Clearly, since the material is isotropic  $E = E_x = E_y$  and  $\nu = \nu_{xy} = \nu_{yx}$

**Table 8:** Identified material parameters

Configurations	$E_x$ [GPa]	$E_y$ [GPa]	$G_{xy}$ [GPa]	$\nu_{xy}$
<b>Configuration #1</b>	2.77	2.77	1.09	0.263
<b>Configuration #2</b>	3.95	1.44	0.94	0.383
<b>Configuration #3</b>	4.17	1.44	1.01	0.307

To verify the validity of the identified parameters, the natural frequencies of the plate have been determined also by FE analysis on ANSYS environment using these aforementioned values. Specifically, for the FE analysis a hexahedral mesh with 395 nodes and 67.000 elements has been used. Pertinent results are shown in Fig. 8, where experimental natural frequencies (black circles) are reported vis-à-vis analytical one [3] (dashed blue line) and numerical FE simulation (magenta squares). In this figure the modes are labelled by two mode indices, namely  $m$  and  $n$ , indicating the number of nodal lines approximately parallel to  $y$ - and  $x$ -axis, respectively, including the boundaries as nodal lines, except when the boundary is free [3]. The frequencies are plotted over the mode index  $m$ . Lines connecting the symbols are guides to the eyes only.

As it can be seen, a very good match between experimental and numerical natural frequencies is achieved, thus proving the validity of the identified parameters. In this regard, a low average relative error between FE results and experimental data, of approximately 2.5%, has been obtained.

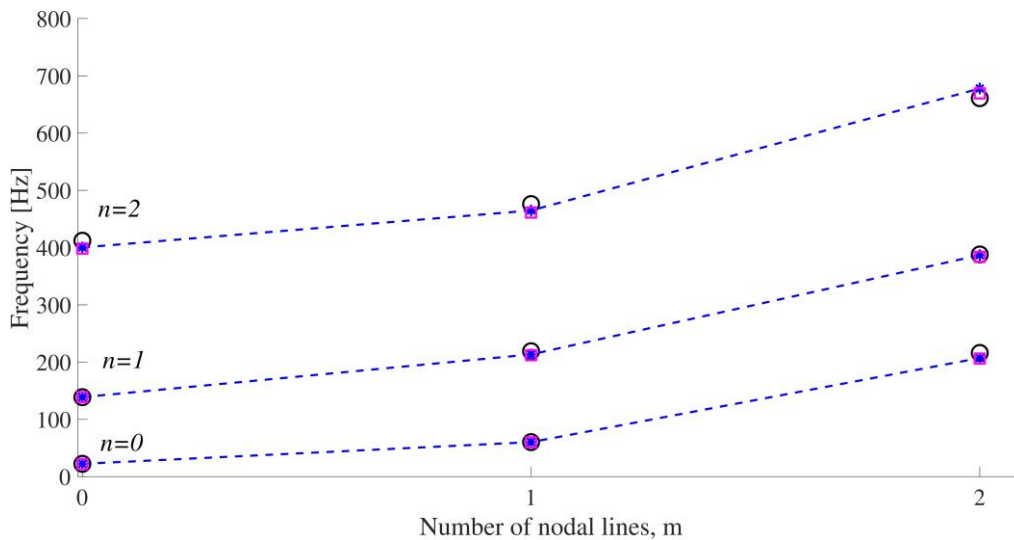


**Figure 8:** Comparison of experimental vis-à-vis numerical data in terms of natural frequencies for Configuration #1. Dashed blue lines –Analytical results; Magenta squares – FE results; Black circles – Experimental data.

Once material parameters of the flat plate (Configuration #1) have been determined and verified, attention has been then focused on the two stiffened plate (Configurations #2 and #3).

Specifically, assuming an orthotropic behavior of these plates, firstly the proposed identification procedure (see Sections 4) has been applied. On this base, equivalent orthotropic parameters of the two Configurations have been retrieved minimizing the functional in Eq. (32) considering the  $n_f = 10$  experimentally determined natural frequencies  $\tilde{\omega}_k$  in Tab. 7. The pertinent identified mechanical parameters are reported in Tab. 8 (second and third lines). Further, numerical results in

terms of mode shapes and natural frequencies for Configurations #2 and #3 have been also obtained applying the previously described pb-2 Rayleigh-Ritz procedure.

Again, to verify the validity of these identified parameters, natural frequencies and mode shapes of the actual stiffened plate have been determined also via FE analyses on ANSYS environment using the actual geometry of the plate (Tab. 6 and Fig. 4(b)). Specifically, the real plates shape (flat plates with stiffeners) have been modelled with 3D elements, assuming the material isotropic with the previously obtained Configuration #1 Young's modulus and Poisson's ratio (see Tab. 8).

In addition, to further assess the reliability of the approach, equivalent orthotropic plate rigidities have been estimated applying the relations of the so-called EPM for stiffened plates, given in [1]-[2]. In this regard, according to the EPM, the orthogonally stiffened plate can be treated as an equivalent flat plate made of orthotropic material. Specifically, for a rectangular plate reinforced by equidistant stiffeners in one direction of thickness  $\tilde{h}$ , disposed symmetrically with respect to the middle plane of the plate (Fig. 4(b)), and assuming that both the plate and the stiffeners are made of the same isotropic material, EPM yields the equivalent rigidities as

$$D_x = \frac{E h^3}{12(1-\nu^2)} + \frac{E I}{(\tilde{p} + \tilde{L})}; \quad D_y = \frac{E h^3}{12(1-\nu^2)}; \quad D_t = \nu D_y; \quad (38)$$

$$\nu_{xy} = \frac{D_t}{D_y}; \quad \nu_{yx} = \frac{D_t}{D_x}; \quad D_t \approx \frac{(1 - \sqrt{\nu_{xy}\nu_{yx}})\sqrt{D_x D_y}}{2}$$

where  $E$  and  $\nu$  are the elastic constant of Configuration #1 given in Tab. 8,  $I$  the moment of inertia of the stiffener taken with respect to the middle axis of the cross section of the plate, while  $\tilde{p}$  and  $\tilde{L}$  are reported in Fig. 4(b). In this manner, based on Eq. (38), Eq. (23) yields the corresponding natural frequencies of Configurations #2 and #3 for the EPM.

Comparisons of the different adopted procedures are shown in Fig.9. In this figure natural frequencies obtained applying the proposed procedure (red dotted line) are compared with the experimentally determined natural frequencies (black circles), the EPM numerical data (dashed blue line) and the numerical FE simulation results (magenta squares).

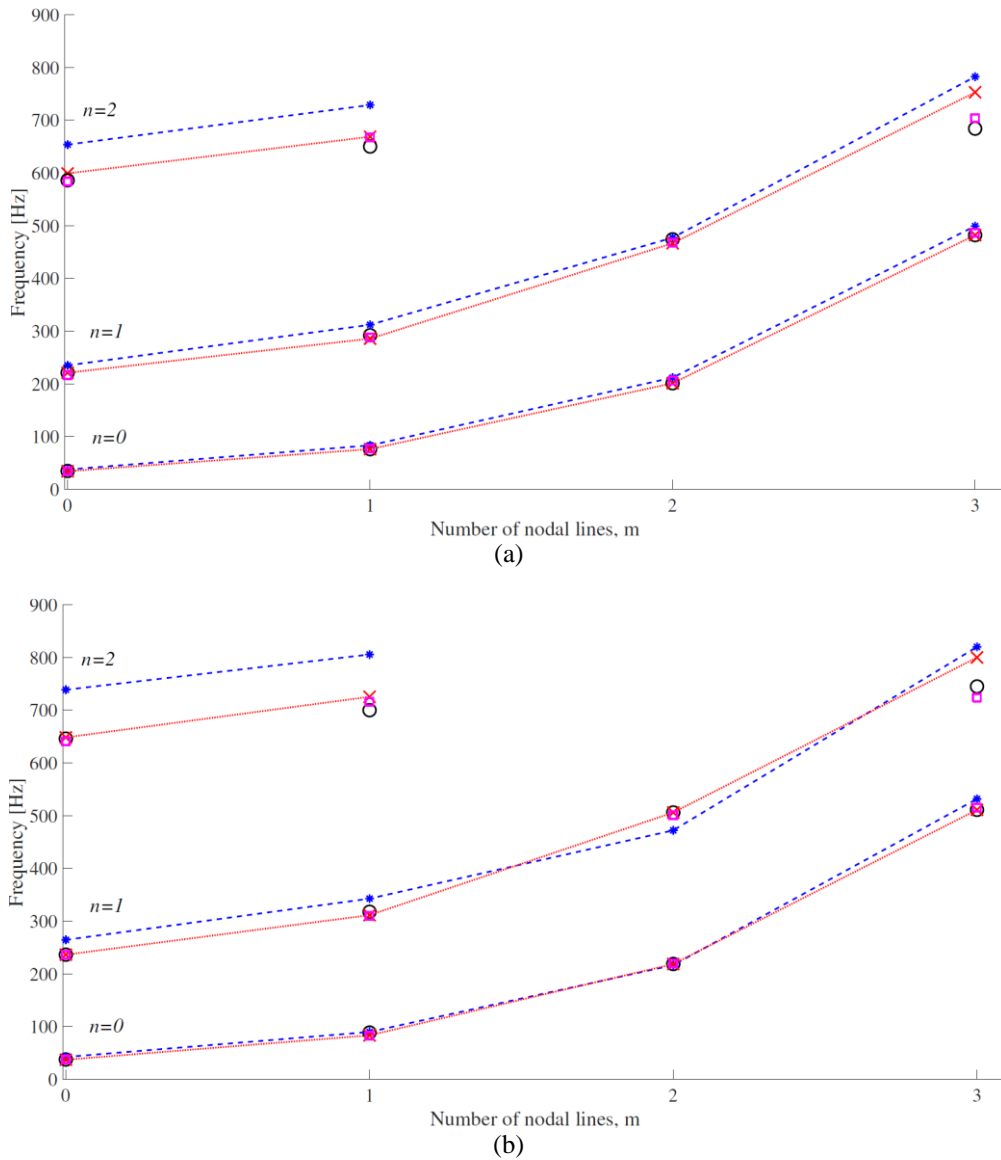


**Figure 9:** Comparison of experimental vis-à-vis numerical data in terms of natural frequencies: a) Configuration #2; b) Configuration #3. Red dotted lines - Proposed procedure results; Blue dashed lines - EPM results; Magenta squares - FE results; Black circles - Experimental data.

As apparent, proposed method results excellently agree with both pertinent experimental data and FE simulations, thus proving the reliability of the proposed identification procedure. Specifically, the average relative errors between proposed method results and experimental data are 2.1% for Configuration #2 and 2.2% for Configuration #3. Moreover, considering that FE analyses have been carried out on the actual plates geometry, thus no assumptions have been made for these simulations, the validity of the applied experimental procedure has been further assessed.

As far as the EPM results are concerned, Fig. 9 shows that EPM leads to a satisfactory agreement with the experimental data at lower frequencies, while, as expected, the accuracy of the EPM results decrease drastically at higher frequencies. It can be therefore argued that EPM could be adopted to estimate the first few natural frequencies of stiffened plates.

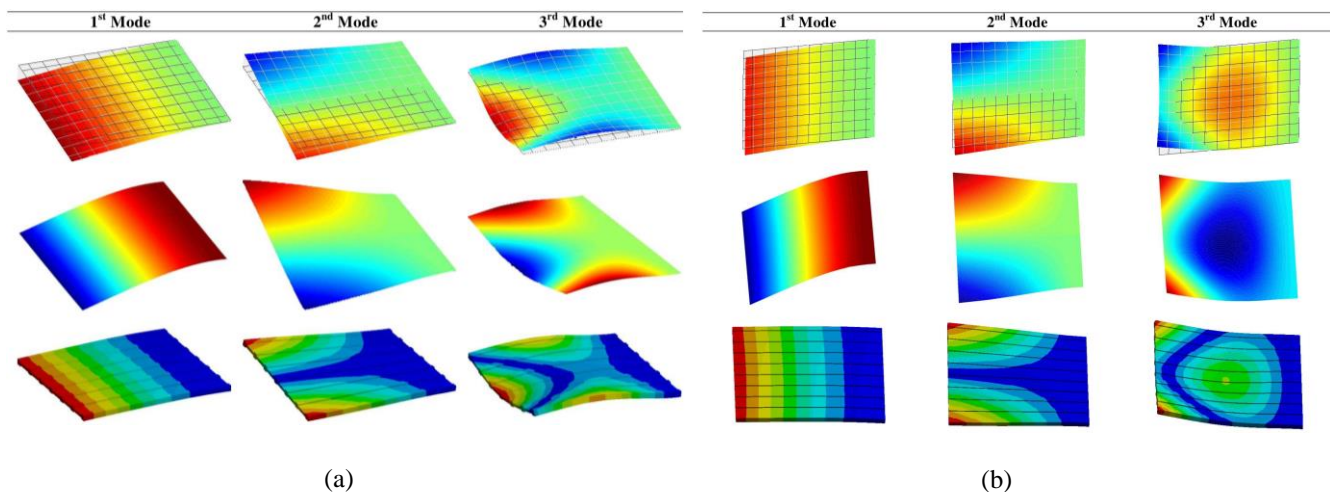


**Figure 10:** Comparison of experimental vis-à-vis numerical results in terms of mode shapes for stiffened plates: a) Configuration #2; b) Configuration #3. First row- Experimental data; Second row – Numerical results with proposed procedure; Third row – FE results with ANSYS.

In addition, as shown in Fig. 10, analogous analyses have been also performed in terms of mode shapes. Specifically, in this figure, the first three mode shapes obtained experimentally are compared with those numerically determined with the proposed procedure and FE analyses with ANSYS on the actual stiffened plate geometry. As it can be observed, these numerical methods lead to satisfactory agreement with the experimental data. Similar results have also been obtained for higher modes, here omitted for brevity's sake.

## Concluding Remarks

In this paper, an innovative identification procedure has been proposed for estimating mechanical properties of orthotropic arbitrarily shaped plates, based on free-vibration data. Plates natural frequencies have been determined resorting to a Rayleigh-Ritz scheme. Specifically, the so-called pb-2 Rayleigh-Ritz approach has been appropriately extended to deal with the case of orthotropic plates. It has been shown that this approach could lead to computationally demanding double integrals in the plate domain. To account for the possibility of employing generic plate shapes, these double integrals have been appropriately converted to more simple line integrals, taking advantage of the Green's theorem. In this manner, numerical double integration can be conveniently circumvented. The procedure has led to a generalized eigenvalue problem for the plate natural frequencies and mode shapes, that involves matrices which explicitly depend on the material elastic constants. This feature has been exploited to yield material properties based on available natural frequencies. In this regard, an appropriate objective function has been introduced and conveniently minimized through the Particle-Swarm Optimization method, allowing to expeditiously identify material parameters. Numerical analyses have been performed for several

plate shapes, as well as different boundary conditions and materials, and comparisons of the proposed method estimated elastic constants have been made with those already presented in the literature. The results have shown a satisfactory agreement between the two solutions, demonstrating the reliability of the proposed approach.

Additionally, an extensive experimental study has been undertaken to assess the accuracy of the procedure. In this regard, considering the obvious relevance for modern additive manufacturing processes, free-vibrations tests have been carried out for several rectangular 3D printed stiffened plates. Specifically, plates have been realized through a fuse deposition modeling 3D printer, employing common polylactic acid filaments. In this manner possible defects related to the bonding between the plate and the stiffeners have been avoided. Experimentally measured frequencies and mode shapes have been obtained using both laser scanning vibrometer and impulsive tests, employing the proposed approach to identify the equivalent orthotropic mechanical properties and corresponding natural frequencies. Moreover, 3D Finite Element analyses of the stiffened plates have been performed as a further reference. Proposed procedure based frequencies considered vis-à-vis pertinent experimental data and FE simulations have assessed the reliability and accuracy of the proposed approach. Furthermore, results of the well-known Equivalent Plate Model, commonly employed to analyze corrugated and stiffened plates as orthotropic ones, have been reported, as well. Data have shown a reasonably good agreement with the experimental and proposed method results for the first modes, while discrepancies have increased at higher modes.

## **Acknowledgement**

Alberto Di Matteo and Antonina Pirrotta gratefully acknowledge the support received from the Italian Ministry of University and Research, through the PRIN 2015 funding scheme (project 2015 JW9NJT - Advanced mechanical modeling of new materials and structures for the solution of 2020 Horizon challenges).

The collaboration of Mr. Andrea Evola for the preparation of the 3D printed plates is also gratefully acknowledged.

## Appendix A

In this Appendix, detailed derivation of Eqs. (23) – (26) is reported for completeness' sake.

In this regard, substituting Eq. (14) into the expressions of the maximum strain and kinetic energy in Eqs. (5) – (6), leads to

$$\begin{aligned} \mathcal{U} = & \frac{1}{2} \iint_{\Omega} \left[ D_x \left( \sum_{j=1}^N c_j \frac{\partial^2 \phi_j}{\partial x^2} \right) \left( \sum_{i=1}^N c_i \frac{\partial^2 \phi_i}{\partial x^2} \right) + 2\nu_{xy} D_y \left( \sum_{j=1}^N c_j \frac{\partial^2 \phi_j}{\partial x^2} \right) \left( \sum_{i=1}^N c_i \frac{\partial^2 \phi_i}{\partial y^2} \right) + \right. \\ & \left. + D_y \left( \sum_{j=1}^N c_j \frac{\partial^2 \phi_j}{\partial y^2} \right) \left( \sum_{i=1}^N c_i \frac{\partial^2 \phi_i}{\partial y^2} \right) + 4D_t \left( \sum_{j=1}^N c_j \frac{\partial^2 \phi_j}{\partial x \partial y} \right) \left( \sum_{i=1}^N c_i \frac{\partial^2 \phi_i}{\partial x \partial y} \right) \right] dx dy \end{aligned} \quad (\text{A.1})$$

and

$$\mathcal{T} = \frac{1}{2} \rho h \omega^2 \iint_{\Omega} \left( \sum_{j=1}^N c_j \phi_j \right) \left( \sum_{i=1}^N c_i \phi_i \right) dx dy \quad (\text{A.2})$$

Taking into account Eq. (21) and performing variation with respect to the unknown coefficients  $c_j$  as in Eq. (22), yields

$$\begin{aligned} & 2D_x \sum_{i,j=1}^N c_i \left( \iint_{\Omega} \frac{\partial^2 \phi_i}{\partial x^2} \frac{\partial^2 \phi_j}{\partial x^2} dx dy \right) + 2\nu_{xy} D_y \sum_{i,j=1}^N c_i \left( \iint_{\Omega} \frac{\partial^2 \phi_i}{\partial x^2} \frac{\partial^2 \phi_j}{\partial y^2} dx dy + \iint_{\Omega} \frac{\partial^2 \phi_i}{\partial y^2} \frac{\partial^2 \phi_j}{\partial x^2} dx dy \right) + \\ & 2D_y \sum_{i,j=1}^N c_i \left( \iint_{\Omega} \frac{\partial^2 \phi_i}{\partial y^2} \frac{\partial^2 \phi_j}{\partial y^2} dx dy \right) + 8D_t \sum_{i,j=1}^N c_i \left( \iint_{\Omega} \frac{\partial^2 \phi_i}{\partial x \partial y} \frac{\partial^2 \phi_j}{\partial x \partial y} dx dy \right) - 2\rho h \omega^2 \sum_{i,j=1}^N c_i \left( \iint_{\Omega} \phi_i \phi_j dx dy \right) = 0 \end{aligned} \quad (\text{A.3})$$

Let introduce the integral in Eq. (24), that is

$$R_{ij}^{(de,pq)} = \iint_{\Omega} \left[ \frac{\partial^{d+e} \phi_i(x,y)}{\partial x^d \partial y^e} \right] \left[ \frac{\partial^{p+q} \phi_j(x,y)}{\partial x^p \partial y^q} \right] dx dy, \quad i=1, \dots, N; j=1, \dots, N \quad (\text{A.4})$$

where the generic superscript  $(de,pq)$  of the term  $R_{ij}^{(de,pq)}$  refers to the order of the partial derivatives of the functions  $\phi_i(x,y)$  and  $\phi_j(x,y)$  at the right-hand side of Eq. (A.4).

In this manner, the integrals in Eq. (A.3) can be specified as

$$\begin{aligned}
R_{ij}^{(20,20)} &= \iint_{\Omega} \left[ \frac{\partial^{2+0} \phi_i}{\partial x^2 \partial y^0} \right] \left[ \frac{\partial^{2+0} \phi_j}{\partial x^2 \partial y^0} \right] dx dy = \iint_{\Omega} \frac{\partial^2 \phi_i}{\partial x^2} \frac{\partial^2 \phi_j}{\partial x^2} dx dy; \\
R_{ij}^{(20,02)} &= \iint_{\Omega} \left[ \frac{\partial^{2+0} \phi_i}{\partial x^2 \partial y^0} \right] \left[ \frac{\partial^{0+2} \phi_j}{\partial x^0 \partial y^2} \right] dx dy = \iint_{\Omega} \frac{\partial^2 \phi_i}{\partial x^2} \frac{\partial^2 \phi_j}{\partial y^2} dx dy; \\
R_{ij}^{(02,20)} &= \iint_{\Omega} \left[ \frac{\partial^{0+2} \phi_i}{\partial x^0 \partial y^2} \right] \left[ \frac{\partial^{2+0} \phi_j}{\partial x^2 \partial y^0} \right] dx dy = \iint_{\Omega} \frac{\partial^2 \phi_i}{\partial y^2} \frac{\partial^2 \phi_j}{\partial x^2} dx dy; \\
R_{ij}^{(02,02)} &= \iint_{\Omega} \left[ \frac{\partial^{0+2} \phi_i}{\partial x^0 \partial y^2} \right] \left[ \frac{\partial^{0+2} \phi_j}{\partial x^0 \partial y^2} \right] dx dy = \iint_{\Omega} \frac{\partial^2 \phi_i}{\partial y^2} \frac{\partial^2 \phi_j}{\partial y^2} dx dy; \\
R_{ij}^{(11,11)} &= \iint_{\Omega} \left[ \frac{\partial^{1+1} \phi_i}{\partial x^1 \partial y^1} \right] \left[ \frac{\partial^{1+1} \phi_j}{\partial x^1 \partial y^1} \right] dx dy = \iint_{\Omega} \frac{\partial^2 \phi_i}{\partial x \partial y} \frac{\partial^2 \phi_j}{\partial x \partial y} dx dy; \\
R_{ij}^{(00,00)} &= \iint_{\Omega} \left[ \frac{\partial^{0+0} \phi_i}{\partial x^0 \partial y^0} \right] \left[ \frac{\partial^{0+0} \phi_j}{\partial x^0 \partial y^0} \right] dx dy = \iint_{\Omega} \phi_i \phi_j dx dy;
\end{aligned} \tag{A.5 a-f}$$

and Eq. (A.3) can be rewritten in more compact form as

$$\begin{aligned}
D_x \sum_{i,j=1}^N c_i R_{ij}^{(20,20)} + v_{xy} D_y \sum_{i,j=1}^N c_i \left( R_{ij}^{(20,02)} + R_{ij}^{(02,20)} \right) + D_y \sum_{i,j=1}^N c_i R_{ij}^{(02,02)} + \\
4D_t \sum_{i,j=1}^N c_i R_{ij}^{(11,11)} - \rho h \omega^2 \sum_{i,j=1}^N c_i R_{ij}^{(00,00)} = 0
\end{aligned} \tag{A.6}$$

Let  $\mathbf{c}$  be the vector containing the unknown coefficients, that is  $\mathbf{c}^T = [c_1 \dots c_N]$ , and  $\mathbf{R}^{(20,20)}$ ,  $\mathbf{R}^{(20,02)}$ ,  $\mathbf{R}^{(02,20)}$ ,  $\mathbf{R}^{(02,02)}$ ,  $\mathbf{R}^{(11,11)}$ , and  $\mathbf{R}^{(00,00)}$ , the matrices containing as elements those in Eqs. (A.5 a) – (A.5 f) respectively. Then, Eq. (A.6) can be rewritten in compact matrix form as

$$\left[ \frac{D_x}{v_{xy}} \mathbf{R}^{(20,20)} + \frac{D_y}{v_{xy}} \mathbf{R}^{(02,02)} + D_y \left[ \mathbf{R}^{(20,02)} + \mathbf{R}^{(02,20)} \right] + 4 \frac{D_t}{v_{xy}} \mathbf{R}^{(11,11)} - \lambda \mathbf{R}^{(00,00)} \right] \mathbf{c} = \mathbf{0} \tag{A.7}$$

where  $\lambda = \rho h \omega^2 / v_{xy}$ .

Finally, recalling Eqs. (25) and (26), that is

$$\mathbf{K} = \frac{D_x}{v_{xy}} \mathbf{R}^{(20,20)} + \frac{D_y}{v_{xy}} \mathbf{R}^{(02,02)} + D_y \left[ \mathbf{R}^{(20,02)} + \mathbf{R}^{(02,20)} \right] + 4 \frac{D_t}{v_{xy}} \mathbf{R}^{(11,11)} \tag{A.8}$$

and

$$\mathbf{M} = \mathbf{R}^{(00,00)} \tag{A.9}$$

the generalized eigenvalue problem in Eq. (23) is retrieved.

## References

- [1] Timoshenko SP, Woinowsky-Krieger S. Theory of plates and shells. New York: MCGraw-Hill, 1959.
- [2] Szilard R. Theories and Applications of Plate Analysis: Classical, Numerical and Engineering Methods. Hoboken: John Wiley & Sons, 2004.
- [3] Leissa A.W. Vibrations of plates (NASA SP-160). Washington, DC: Government Printing Office, 1969.
- [4] Lekhnitskii SG. Anisotropic plates. New York: Gordon and Breach, 1968.
- [5] Bedair O. Analysis and limit state design of stiffened plates and shells: a world view. Appl Mech Reviews 2009; 62:020801.
- [6] Xing YF, Liu B. New exact solutions for free vibrations of thin orthotropic rectangular plates. Comp Struct 2009; 89:567-574.
- [7] Biancolini ME, Brutti C, Reccia L. Approximate solution for free vibrations of thin orthotropic plates. J Sound Vib 2005; 288:321-344.
- [8] Abrate S. Free vibration, buckling, and static deflections of functionally graded plates. Comp Sci Technol 2006; 66:2383-2394.
- [9] Kennedy D, Cheng RKH, Wei S, Alcazar Arevalo FJ. Equivalent layered models for functionally graded plates. Comput Struct 2016; 174:113-121.
- [10] Zhang DG, Zhou YH, A theoretical analysis of FGM plate based on physical neutral surface. Comput Mater Sci 2008; 44:716–720.
- [11] Bhat RB. Natural frequencies of rectangular plates using characteristic orthogonal polynomials in the Rayleigh–Ritz method. J Sound Vib 1985;102:493-499.
- [12] Dickinson SM, Di Blasio A. On the use of orthogonal polynomials in the Reyleigh–Ritz method for the study of the flexural vibration and buckling of isotropic and orthotropic rectangular plates. J Sound Vib 1986;108:51–62.
- [13] Tsay CS, Reddy JN. Bending, stability and free vibrations of thin orthotropic plates by simplified mixed finite elements. J Sound Vib 1978; 59:307-311.
- [14] AL-Khaiat H. Free vibration analysis of orthotropic plates by the initial value method. Comput Struct 1989; 33:1431–1435.
- [15] Chen YZ. Evaluation of fundamental vibration frequency of an orthotropic bending plate by using an iterative approach. Comput Methods Appl Mech Eng 1998; 161:289-96.
- [16] Bardell NS, Dunsdon JM, Langley RS. Free vibration analysis of thin coplanar rectangular plate assemblies – Part I: theory, and initial results for specially orthotropic plates. Compos Struct 1996; 34:129-143.

- [17] Kim CS. Natural frequencies of orthotropic, elliptical and circular plates. *J Sound Vib* 2003; 259:733-745.
- [18] Kim CS., Dickinson SM. The free flexural vibration of isotropic and orthotropic general triangular shaped plates. *J Sound Vib* 1992: 383-403.
- [19] Farag AM, Ashour AS. Free vibration of orthotropic skew plates. *J Vib Acoustic* 2000; 122:313-317.
- [20] Liew KM, Lam KY. A Rayleigh-Ritz approach to transverse vibration of isotropic and anisotropic trapezoidal plates using orthogonal plate functions. *Int J Solids Struct* 1991; 27:189-203.
- [21] Carlsson LA, Pipes RB. Experimental characterization of advanced composite materials. New York: Prentice-Hall, 1987.
- [22] Moussu F, Nivoit M. Determination of elastic constants of orthotropic plates by a modal analysis/method of superposition. *J Sound Vib* 1993; 165:149-163.
- [23] Deobald LR, Gibson RF. Determination of elastic constants of orthotropic plates by a modal analysis/Rayleigh-Ritz technique. *J Sound Vib* 1988; 124:269-283.
- [24] Mota Soares CM, Moreira de Freitas M, Araujo AL, Pedersen P. Identification of material properties of composite plate specimens. *Composite Struct* 1993; 25:277-285.
- [25] Larsson D. Using modal analysis for estimation of anisotropic material constants. *J Eng Mech* 1997; 123:222-229.
- [26] Cunha J, Cogan S, Berthod C. Application of genetic algorithms for the identification of elastic constants of composite materials from dynamic tests. *Int J Numer Methods Eng* 1999; 45:891-900.
- [27] Rikards R, Chate A, Steinchen W, Kessler A, Bledzki AK. Method for identification of elastic properties of laminates based on experiment design. *Compos Pt B-Eng* 1999; 30:279-289.
- [28] Hwang SF, Chang CS. Determination of elastic constants of materials by vibration testing. *Compos Struct* 2000; 49:183-190.
- [29] Chakraborty S, Mukhopadhyay M, Sha OP. Determination of physical parameters of stiffened plates using genetic algorithm. *J Comput Civ Eng* 2002; 16:206-221.
- [30] Maletta C, Pagnotta L. On the determination of mechanical properties of composite laminates using genetic algorithm. *Int J Mech Mat Design* 2004; 1:199-211.
- [31] Hwang SF, Wu JC, He RS. Determination Identification of effective elastic constants of composite plates based on a hybrid genetic algorithm. *Compos Struct* 2009; 90: 217-224.
- [32] Daghia F, De Miranda S, Ubertaini F, Viola E. Estimation of elastic constants of thick laminated plates within a Bayesian framework. *Compos Struct* 2007; 80:461-473.

- [33] Auzins J, Chate A, Rikards R, Skukis E. Metamodeling and robust minimization approach for the identification of elastic properties of composites by vibration method. *ZAMM-Z Angew Math Mech* 2015; 10:1012-1026.
- [34] Liew KM, Wang CM. pb-2 Rayleigh-Ritz method for general plate analysis. *Eng Struct* 1993; 15:55-60.
- [35] Liew KM. Response of plates of arbitrary shape subject to static loading. *J Eng Mech* 1992; 118:1783-1794.
- [36] Liew KM. Vibration analysis of plates by the pb-2 Rayleigh-Ritz method: mixed boundary conditions, reentrant corners, and internal curved supports. *Mech Struct Mach* 1992; 20:281-292.
- [37] Milazzo A., Oliveri V. Post-buckling analysis of cracked multilayered composite plates by pb-2 Rayleigh-Ritz method. *Compos Struct* 2015; 132: 75-86
- [38] Kennedy J, Eberhart R. Particle swarm optimization. In: *Proceedings of IEEE International Conference on Neural Networks*. Perth, November, 1995. Vol. IV p. 1942-1948.
- [39] Perez RE, Behdinan K. Particle swarm approach for structural design optimization. *Comput Struct* 2007; 85:1579-1588.
- [40] Plevris V, Papadrakakis M. A hybrid particle swarm-gradient algorithm for global structural optimization. *Comput-Aided Civil Infrastruct Eng* 2011; 26:48–68.
- [41] Di Matteo, A., Lo Iacono, F., Navarra, G., Pirrotta, A. Direct evaluation of the equivalent linear damping for TLCD systems in random vibration for pre-design purposes. *Int J Non-Linear Mech* 2014; 63: 19-30.
- [42] Di Matteo A, Furtmuller T, Adam C, Pirrotta A. Optimal design of tuned liquid column dampers for seismic response control of base-isolated structures. *Acta Mech* 2018; 229:437-454.
- [43] Dorigo M, Maniezzo V, Colorni A. The ant system: optimization by a colony of cooperating agents. *IEEE Trans Syst Man Cybern Part B-Cybern* 1996; 26:29-41.
- [44] Cottone G, Fileccia Scimemi G, Pirrotta A.  $\alpha$ -stable distributions for better performance of ACO in detecting damage on not well spaced frequency systems. *Probab Eng Mech* 2014; 35: 29-36.
- [45] Grediac M, Paris PA. Direct identification of elastic constants of anisotropic plates by modal analysis: theoretical and numerical aspects. *J Sound Vibr* 1996; 193:401-415.
- [46] Kim CG, Hong CS. Buckling of unbalanced anisotropic sandwich plates with finite bending stiffness. *AIAA J* 1988; 26:982-988.

- [47] Aoki Y, Maysenhölder W. Experimental and numerical assessment of the equivalent-orthotropic-thin-plate model for bending of corrugated panels. *Int J Solids Struct* 2017; 108:11-23.
- [48] Huffington NJ. Theoretical determination of rigidity properties of orthogonally stiffened plates. *J Appl Mech* 1956; 26:15-20.
- [49] Hoppman HW, Huffington NJ, Magness LS. A Study of Orthogonally Stiffened Plates, *J Appl Mech* 1956; 23:243-250.
- [50] Hoppmann WH, Baltimore M. Bending of Orthogonally Stiffened Plates, *J Appl Mech* 1955; 22: 267-271.
- [51] Hoppmann WH, Magness LS, Baltimore M. Nodal patterns of the free flexural vibrations of stiffened plates. *J Appl Mech* 1956; 22:526-530
- [52] Luan Y, Ohlrich M, Jacobsen F. Improvements of the smearing technique for cross-stiffened thin rectangular plates. *J Sound Vib* 2011; 330:4274-4286.